Appl Phys A (2010) 99: 363–375
DOI 10.1007/s00339-010-5673-5

Applied Physics A
Materials Science & Processing

Degradation of azurite in mural paintings: distribution of copper carbonate, chlorides and oxalates by SRFTIR

A. Lluveras · S. Boularand · A. Andreotti · M. Vendrell-Saz

Received: 19 January 2010 / Accepted: 1 March 2010 / Published online: 9 April 2010

Abstract This article illustrates the analysis by synchrotron micro-analytical techniques of an azurite painting presenting greenish chromatic degradation. The challenge of the experiments was to obtain the spatial distribution of the degradation products of azurite. Copper hydroxychlorides, carbonates and copper oxalates have been mapped by SR FTIR imaging of cross sections in transmission mode. To complement the information, Py/GC/MS and GC/MS techniques were applied in order to characterize the binding media and organic materials present as well as their degradation products. Results contribute to a better understanding of the decay of blue areas in ancient paintings not only from the particular point of view of azurite weathering, but also by adding information regarding the oxalates' formation and their distribution in painting samples. Synchrotron radiation demonstrates its capability for the mapping in painting cross sections.

1 Introduction

Azurite is a basic copper carbonate ($2CuCO_3{\cdot}Cu(OH)_2$), a natural blue pigment used since the Fourth Dynasty in Egypt although it became the most important blue pigment during the Middle Ages and Renaissance [1].

A. Lluveras (✉) · S. Boularand · M. Vendrell-Saz
Departament de Cristal·lografia, Mineralogia i Dipòsits Minerals, Universitat de Barcelona, C/Martí i Franquès S/N, 08028 Barcelona, Spain
e-mail: alluveras@ub.edu
Fax: +34-934-021340

A. Andreotti
Dipartimento di Chimica e Chimica Industriale, Università di Pisa, Via Risorgimento 35, Pisa, Italy

Many paintings became altered by the transformation of blue areas into green and brown. Clear examples of the problematic above described are the frescoes at the Monumental Cemetery of Pisa or the Crypt of the Cathedral of Siena [2, 3].

Green shades in azurite blue paintings could be attributed to different reasons depending on their composition: natural green shades of the mineral ore, the use of synthetic green pigments obtained from the corrosion of copper plates exposed to vinegar vapours, or the degradation of the original pigment into green products such as copper chlorides.

Although azurite presents a natural greenish undertone due to the particles of malachite ($CuCO_3{\cdot}Cu(OH)_2$) and cuprite (Cu_2O) that can be found associated in nature to the azurite ores [1], the desiderated blue tone could be obtained by purification of azurite from the other phases as it was provided by authors such as Cennino Cennini [4]. Though the synthesis of green copper-based pigments have been reported in recipes of Heraclius, Teophilus or Vitruvius [5, 6], the synthesis process products have been already characterized as mixtures of copper acetates, carbonates and hydroxychlorides [7], that is, a different composition from that of the green shaded azurite-based paintings usually characterized in the literature.

Thus, degradation of azurite blue pigment into a green product due to ageing seems to be the cause of the greenish areas observed in different azurite paintings as the ones cited above. Azurite, although being stable to light and atmosphere, presents frequent chromatic alterations to greenish tonalities due to transformation into paratacamite and atacamite ($Cu_2Cl(OH)_3$) [2, 3, 8, 9] and also malachite ($CuCO_3{\cdot}Cu(OH)_2$) [1], not yet completely understood.

Samples analyzed come from a gypsum shield on top of a door in the Monastery of Santes Creus (Catalonia, Spain) dating from the 1605 AD. The shield is depicted mainly in

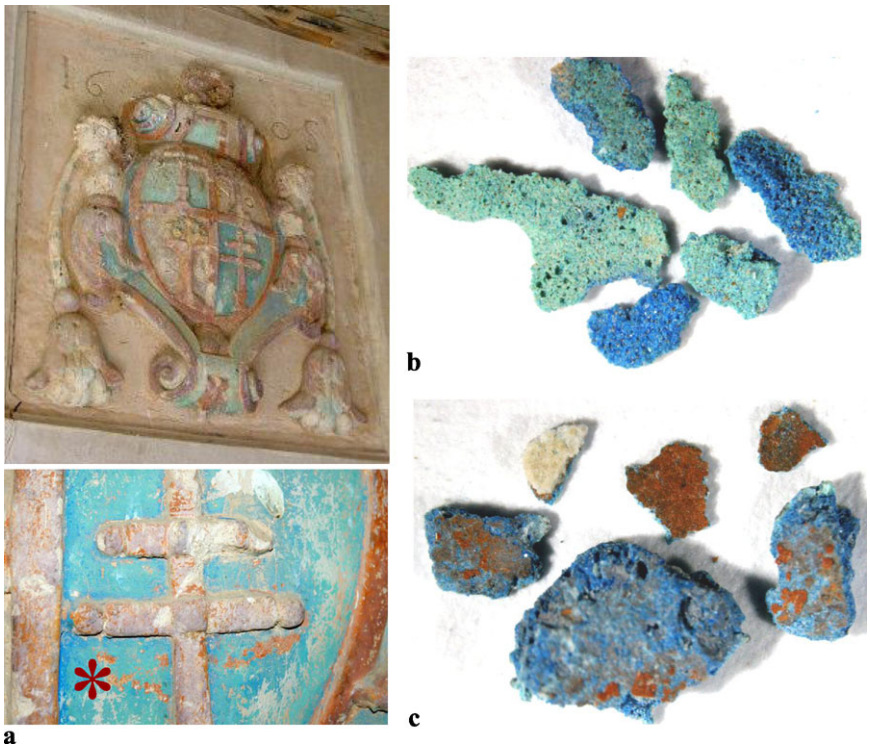

Fig. 1 (**a**) Sampled shield. *Red asterisk* marks the sampling point in the *blue area*; several fragments of the sample of different characteristics: (**b**) *blue* and *green shades*; (**c**) fragments showing the *brown layer*

blue and brown in order to underline the relieves with the monastery insignias. In the blue areas, green shades could easily be identified (Fig. 1a).

Synchrotron radiation X-ray diffraction and synchrotron IR microscopy have been used to produce maps of phases and high contrast chemical imaging. Experiments were performed at the European Synchrotron Radiation Facility (ESRF, Grenoble, France) at the station ID 21. Results helped to unequivocally characterize the inorganic crystalline products formed by the weathering process of azurite and also to determine the distribution of those products along the blue layer. Thus, experiments constitute a significant contribution to better understand the chromatic degradation of azurite blue layers and the mechanism of formation of the decay by products. Moreover, experiments add information to the long time discussed mechanisms of the formation of oxalates in mural paintings. Finally, the potentiality and the limits of the synchrotron radiation micro imaging techniques on this kind of samples and the complementary of the information of the techniques used to solve cultural heritage problems will be discussed.

2 Results

2.1 Experimental layout

2.1.1 Microscopy

Samples were preliminarily observed by means of a low magnification stereo-microscope (Nikon SMZ 1500) in order to observe the number and sequence of painting layers including the support and the surface state.

Several fragments of the sample were embedded in polyester resin using methyl ethyl ketone peroxide as hardener (Cronolita E.I., Spain), cut with a low deformation diamond saw and polished to allow the study of the cross section under a reflecting dark field optical microscope. A Nikon Eclipse LV 100 PDL analytical microscope equipped with a Nikon Digital Camera DMX 1200 F was used for visible light microscopy of the polished cross sections.

SEM images of the same sections were taken using a JEOL (Tokyo, Japan) JSM-840 (secondary and backscattered electron detection) with a LINK AN 10000 microanalyzer. The acceleration voltage used was 20 keV.

2.1.2 Fourier Transform Infrared Spectroscopy (FTIR)

Analyses were made with a BOMEM MB-120 Fourier transform infrared spectrometer in two transmission modes, microscope and diamond cell. All results were processed with GRAMS/32 (Galactic) software.

When working with the diamond cell, the equipment was an infrared spectrometer Bomem MB-120 equipped with a potassium bromide beamsplitter and deuterated triglycine sulphate (DTGS) detector. The spectra are the sum of 30 scans collected from 4000 to 350 cm^{-1} at a resolution of 4 cm^{-1}.

Bomem MB-120 Fourier Transform Infrared Spectrometer, equipped with a Spectra-Tech Analytical Plan microscope, was used with the diamond cell, as sample holder.

The spectrometer has a KBr beamsplitter and a Globar source. The microscope has its own mercury cadmium telluride (MCT) detector refrigerated with liquid nitrogen. The spectrum was recorded between 4000 and 720 cm^{-1} with a resolution of 4 cm^{-1} and an accumulation of 100 scans.

2.1.3 Gas chromatography—mass spectrometry

- Pyroprobe CDS Analytical Inc. 5000 Series (Oxford, USA). It was operating with an initial temperature of 50°C, up to 550°C at 20°C/ms, then isothermal for 20 sec. (probe run time 0.33 min). The pyrolyzer was coupled online with the injection port of a GC System Gas Chromatograph, coupled with a Mass Detector. The interface temperature of the pyrolyzer was 180°C, the transfer line 300°C, the valve oven 290°C. A few µg of the samples admixed with 2 µl of hexamethyldisilazane were inserted into a quartz tube and placed into the pyrolysis chamber.
- 6890N GC System Gas Chromatograph (Agilent Technologies, Palo Alto, CA, USA), coupled with a 5973 Mass Selective Detector (Agilent Technologies, Palo Alto, CA, USA) single quadrupole mass spectrometer, equipped with split/splitless injector. The mass spectrometer was operating in the electron impact (EI) positive mode (70 eV). The MS transfer line temperature was 280°C; the MS ion source temperature was kept at 230°C; and the MS quadrupole temperature was at 150°C. This instrument was used for the Py/GC/MS analyses. Detailed working conditions are published elsewhere [10].
- A 6890N GC System Gas Chromatograph (Agilent Technologies, Palo Alto, CA, USA), coupled with a 5975 Mass Selective Detector (Agilent Technologies, Palo Alto, CA, USA) single quadrupole mass spectrometer, equipped with a PTV injector was used. The mass spectrometer parameters correspond to the ones reported above. This instrument was used for the analysis of samples processed with the combined analytical procedure for the simultaneous identification of glycerolipids, proteinaceous materials, plant and animal resins, and natural waxes. The detailed operating conditions, and the analytical procedure are published in detail elsewhere [11].
- Microwave oven model MLS-1200 MEGA Milestone (FKV, Sorisole (BG,) Italy).

2.1.4 Synchrotron radiation microanalysis

Synchrotron radiation Fourier transform infrared microspectroscopy (SR FTIR) in transmission mode was performed at the station ID21 at the European Radiation Synchrotron Facility (ESRF, Grenoble). Maps were recorded using 4 micron step and 40 scans for each spectrum. Aperture and resolution were fixed at 8 × 8 µm and 8 cm^{-1}, respectively. In all cases the aperture and the step size chosen generate overlapping areas in order to increase the resolution of the components. A microtome Ultracut E with a glass knife was used to obtain slices around 10 µm for the FTIR analysis in transmission mode. Synchrotron radiation experiments conditions are summarized in Table 1.

Table 1 Synchrotron radiation micro-analytical experiments conditions at ESRF station ID21

	SR FTIR (ID21)
λ	3500–900 cm^{-1}
Step size	4 µm
Spot size (aperture)	8 × 8 µm
Resolution	8 cm^{-1}
Slice width	10 µm

2.2 Sample characterization

Samples were characterized by optical observations, and SEM-EDS, FTIR and mass spectrometric-based techniques analysis. Results of the 'conventional' characterization of the sample are reported in Table 2.

2.2.1 Optical microscope

Samples taken from the blue sampling area in the bottom right side of the shield indicated in Fig. 1a, present different characteristics under the stereomicroscope. Some of the fragments present a blue color while others are completely greenish (Fig. 1b). Moreover, some of the fragments exhibit other layers such as a white and a brownish one (Fig. 1c).

A cross section (Fig. 2a) clearly evidences the presence of different layers in one of the sample: a white preparation layer (layer 1), a brown pigment layer (layer 2) and the blue layer of interest (layer 3), corresponding to the layers observed under the stereomicroscope. The fractured appearance and the irregular size (from 5 to 20 µm) of the blue particles as well as the deep blue color in coarse particles while finer particles display pale blue hue in layer 3 are characteristic of azurite [1]. In this sample no green shades were observed.

Figure 2b shows the cross section of another embedded fragment consisting in the blue layer (layer 3) only, without the other layers that formed the complete stratigraphy. In this fragment is appreciable the presence of a matrix with green shades and the existence of blue particles in between.

2.2.2 Scanning Electron Microscope

The same polished samples were carbon coated to be studied under the Scanning Electron Microscope (SEM) with a coupled Energy Dispersive X-ray Spectroscopy (EDS) facility.

Table 2 Summary of the results obtained by means of 'conventional' techniques

Layer number	Color	Thickness (μm)	Layer description	EDS	FTIR	PY-GC/MS	GC/MS
4	Grey	5–6	Superficial patina	Pb	Lead white	–	–
3	Green-blue	50	Pigment layer	Cu, Cl	Azurite Copper Hycroxychlorides Oxalates	Polysaccharide material	Egg Animal fat
M	–	2.5	Metallic leave	Ag	–		–
2	Brown	10	Pigment layer Mordant (adhesive layer of metallic leaf)	Si, Al, Ca, Fe, Ti, Cl, P, S	Clay Iron oxides oxalates	Polysaccharide material	–
1	White	100	Preparation layer	Ca, S	Gypsum Calcium oxalates	–	–

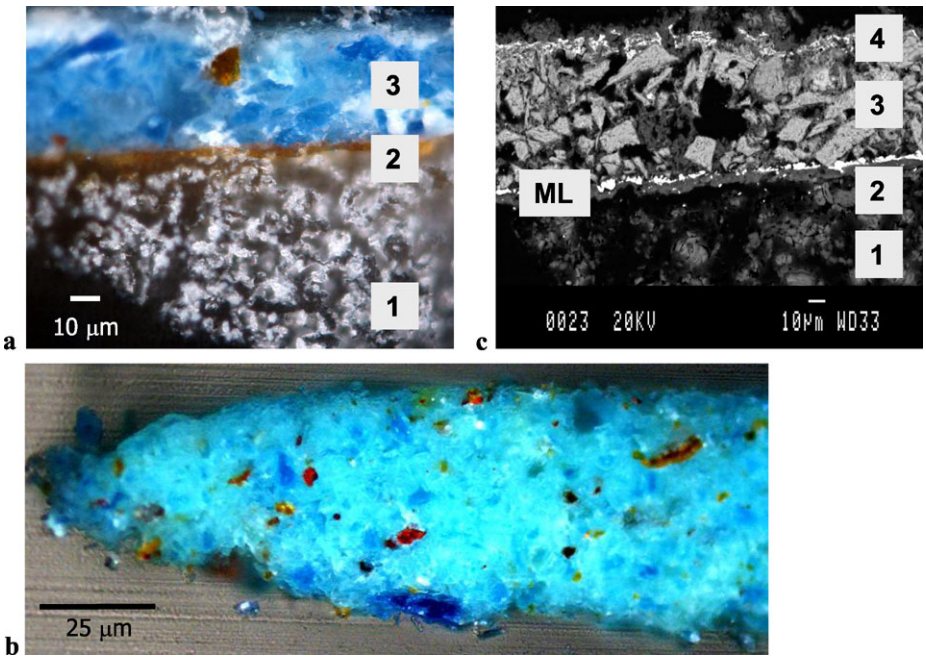

Fig. 2 Cross sections of the sample: (**a**) optical microscope image: 3 layers can be easily appreciated; (**b**) *green shades* of the matrix and the *blue particles* in between can be noticed; (**c**) backscattered SEM image: a superficial layer (layer 4) and a metallic leaf (ML) between layer 2 and 3 are shown

SEM images underline the different morphological characteristics of the layers. The same three layers already characterized by optical microscope (see Sect. 2.2.1) can be also easily identified in backscattered electron images (Fig. 2c). Moreover, a metallic leaf of about 2.5 microns thick (between layers 2 and 3) and a superficial whitish layer on top of the blue one (layer 4) can also be appreciated with this technique.

The chemical elements forming layer 1 detected by EDS (Ca, S) can be probably attributed to calcium sulphate ($CaSO_4 \cdot nH_2O$), which agrees with its morphology of the layer characteristic of gypsum [12, 13]. The main elements detected in layer 2 (Si, Al, Ca, Fe) can be easily attributed to the presence of a clay with iron oxides [13–15]. The P and S also detected in layer 2 could be attributed to an organic material present as binding media in this layer [16].

The blue pigment layer (layer 3) is characterized by the presence of Cu and by the broken appearance and the big size (from 5 to 20 μm) of some of the pigment particles. Those results are consistent with the use of a copper pigment such as azurite [1]. Chlorine (Cl) and copper (Cu) were detected in the greenish fragment of Fig. 2b.

The metallic leave is made of silver (Ag). Finally, in the white superficial layer (layer 4) the presence of Pb can probably be attributed to the presence of a lead compound such as lead white ($2PbCO_3 \cdot Pb(OH)_2$).

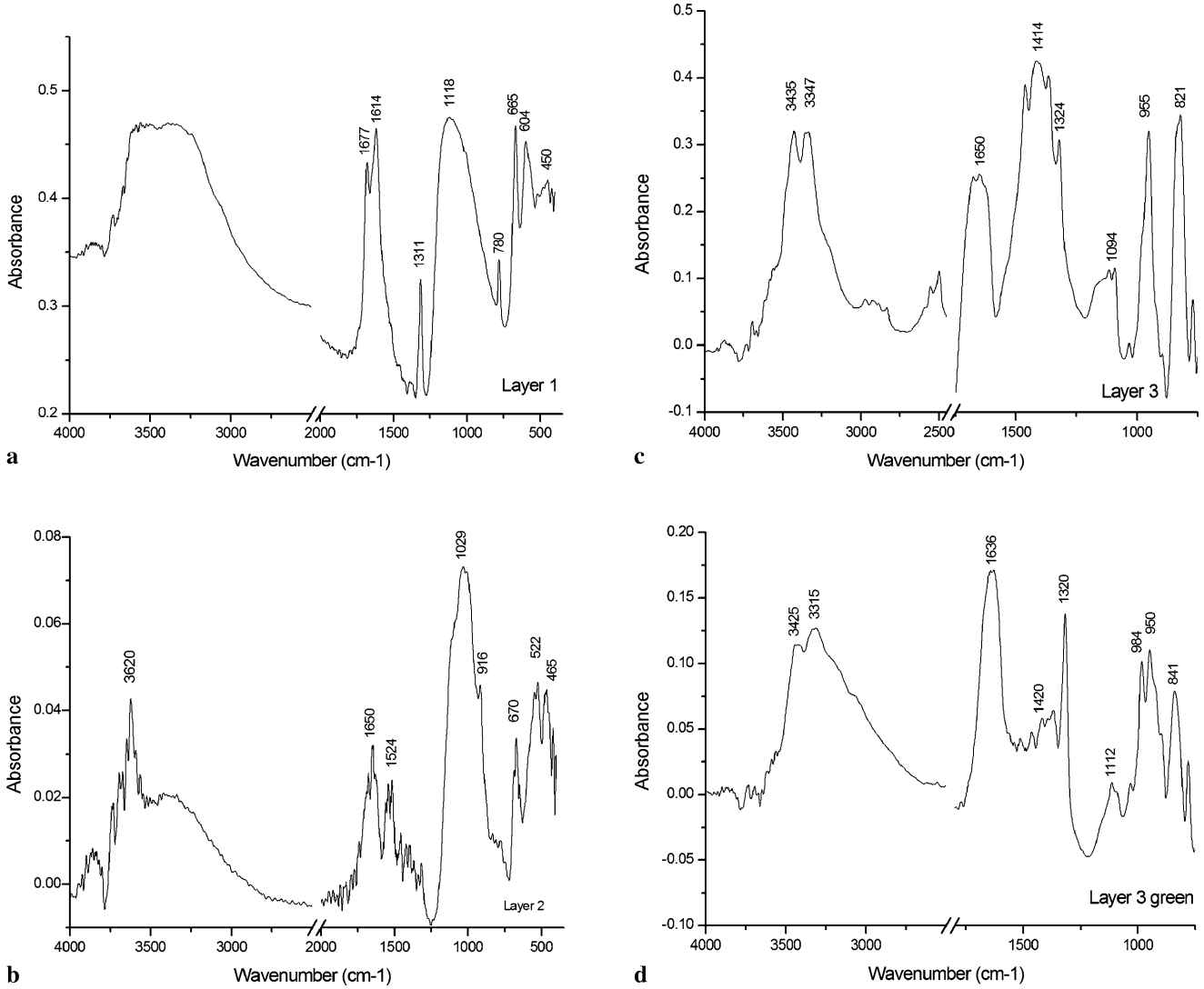

Fig. 3 FTIR spectra of the different layers of the sample (**a**) layer 1; (**b**) layer 2 and (**c**) layer 3; (**d**) selection of *green particles* from layer 3. Conditions: 30 scans, 4 cm^{-1} resolution

Table 3 FTIR bands detected in the different layers of the sample by transmission in a diamond cell

Layer	Detected bands (cm^{-1})
3 blue-green	3428, 3342, 1638, 1316, 1115(b), 1034, 987, 947, 833, 779
3 blue	3428, 3309, 2557, 2505, 1638, 1464, 1403, 1370, 1329, 1115 (b), 1095, 1034, 960, 894, 833, 773, 505, 458, 403
2	3697, 3620, 1650 , 1540 , 1416 , 1315 , 1100, 1022, 916, 542, 472
1	1683, 1620, 1313, 1114, 1004, 779, 669, 596, 463

2.2.3 Fourier Transform Infrared Spectroscopy

Remaining fragments of the sample were analyzed by Fourier Transform Infrared Spectroscopy (FTIR) in transmission mode using a diamond cell. Particles of each layer were isolated by using a dissecting knife and tungsten needles under a stereo-microscope [17]. This way, information on the different layers was obtained separately. Some characteristic spectra of the different layers are presented in Fig. 3. Table 3 presents the bands characteristic of each spectra obtained while Table 4 shows the characteristic bands of the reference materials identified.

In layer 1, the bands at 1683, 1620, 1315, 1114 (broad), 1004, 779, 669, 598 and 463 cm^{-1} correspond to gyp-

Table 4 Transmission reference FTIR characteristic bands of materials

Azurite $2CuCO_3{\cdot}Cu(OH)_2$	Atacamite $Cu_2Cl(OH)_3$	Paratacamite $Cu_2Cl(OH)_3$	Weddellite $CaC_2O_4{\cdot}2H_2O$	Wewellite $CaC_2O_4{\cdot}H_2O$	Copper oxalates $CuC_2O_4{\cdot}nH_2O$	Gypsum $CaSO_4{\cdot}2H_2O$	Spurr (epoxy embedding medium)
				3483		3541	3531
	3443	3448					3467
3425 (s)				3425	3423 (w)	3403	
	3341	3354		3336			
		3322 (sh)					
				3256			
				3061			
							2960
							2935
							2872
							1736
						1684 (sh)	
			1645 (s)		1644 (vs)		1669
				1623 (s)		1619	
1496 (s)							
1465(m)							1457
1416 (s)							1412
				1378 (vw)	1364 (s)		1378
			1321 (s)	1321 (s)	1321 (m)		1345
						1169	1256
1092(m)						1089	1159
							1047
	985	981					
951	950	951					
	915	920	920 (vw)				
	897	897		880(vw)			
	849	847					
831		832			825 (m)		
769			780 (m)	782(m)			
742							
				666		671	
	595	590	618 (w)	591		604	
	515	515	526	515			
497	480	476			502		
457	448					462	

(vs) very strong; (s) strong, (m) medium; (w) weak; (vw) very weak; (sh) shoulder

sum ($CaSO_4{\cdot}2H_2O$) and calcium oxalates ($CaC_2O_4{\cdot}nH_2O$) [12, 13, 19–21].

Layer 2 is characterized by the presence of the peaks at 3697 and 3620 cm^{-1}(OH st), a broad band around 1022 cm^{-1}, with a shoulder at 1100 cm^{-1} (Si–O st), and a peak at 916 cm^{-1}(Al–O–H bd). These peaks can be attributed to a clay, probably kaolinite by the characteristic OH st bands [18, 19].

The presence of the bands centered at 522 and 465 cm^{-1} can be interpreted as iron oxides characteristic peaks. The bands of iron oxides centred at 560 and 480 cm^{-1} can differ by up to 30 cm^{-1} due to differences in particle size and shape of the pigment particles [14], the presence of Fe detected by EDS would corroborate the assignment of these bands.

Oxalate peaks are also present in this layer (layer 2): C=O st at 1620 cm^{-1}, C–O st at 1320 cm^{-1} and C–C st at 780 cm^{-1} are indicative of calcium oxalates [20]. Not well defined bands around 1650, 1530 and 1400 cm^{-1} could be indicative of the presence of a proteinaceous binder (C=O st Amide I, Amide II and C–N st, respectively) [19]. The noisy of those bands does not allow a clear identification.

Blue particles in layer 3 present the characteristic peaks of azurite confirming the identification of the pigment by means of microscope observations (optical and electronical) and EDS results [1]. Azurite characteristic peaks at 3430 (OH st), 1460 and 1414 (CO st), 1092 and 955 (OH bd), 837 and 769 (CO bd), cm^{-1}, are clearly identifiable in the spectra of layer 3 in Fig. 3 [22].

Green particles in layer 3, present both azurite characteristic peaks (cited above) and copper hydroxychlorides (atacamite and paratacamite) bands: 3440 and 3322 (OH st), 986, 948, 896 cm^{-1} [9]. The presence of the characteristic peaks of copper oxalates such as 1644, 1364 and 1321 cm^{-1} (reported above), can be also appreciated allowing the identification of copper oxalates together with copper hydroxychlorides.

2.2.4 Gas chromatography mass spectrometry techniques

For the characterization of the organic materials present in the sample, gas-chromatographic mass spectrometric techniques were applied.

Py/GC/MS results of layer 2 and layer 3 (both blue particles and green particles separately) highlighted the presence of a polysaccharide material by the identification of the characteristic markers: tri-(O-TMS)-levoglucosane and 1,2,3,5-tetrakis-(O-TMS)-xylofuranose and others unknown polysaccharides compounds (evidenced in Fig. 4c and 4d) [23].

In Fig. 4 are also reported for comparison the extracted ion chromatograms of the ions with m/z 217 of the reference materials cherry gum a) as an example of fruit gum, and starch b). Both the green and blue samples present the main pyrolysis product of glucose-based polymers (as an example starch is reported in Fig. 4b). Moreover 1,2,3,5-tetrakis-(O-TMS)-xylofuranose (peak 1), absent in the pyrogram of starch, has been identified in both the samples, suggesting the simultaneous presence of a fruit gum.

GC/MS results were achieved by using the combined procedure already described in literature that allows the identification of lipids, waxes, proteins, and resinous materials in the same microsample [11]. Layer 2 and layer 3 were again analyzed separately. Purification of layer 3 fragments was necessary due to the presence of azurite. Copper-based pigment can form aggregates with the proteinaceous material; in this way some derivatisation problems occur. A solid phase column was used to avoid derivatisation problems as described in literature [24].

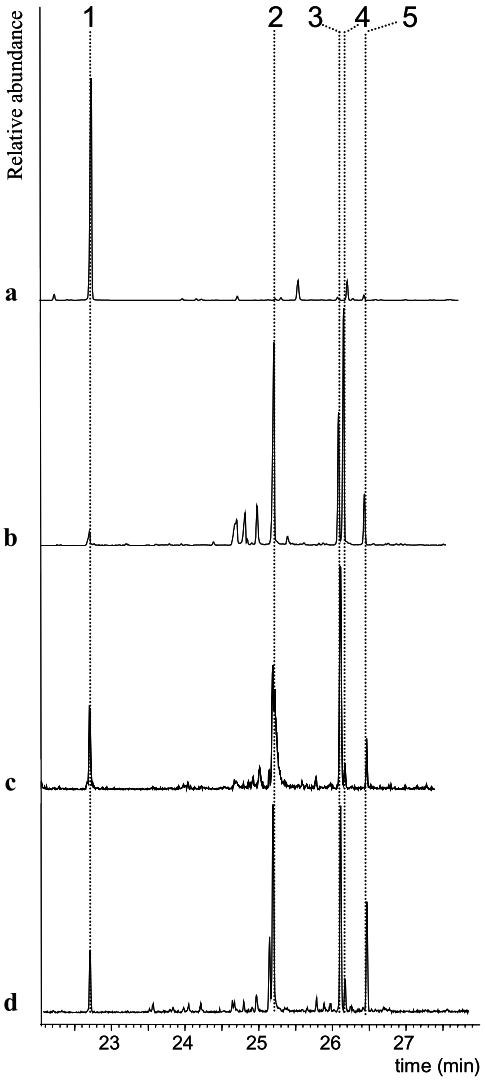

Fig. 4 Extracted chromatograms of the ions with m/z 217 of the reference materials cherry gum (**a**), starch (**b**) compared with the green layer (**c**) and blue layer (**d**) of sample E1: peak 1 = 1,2,3,5-tetrakis-(O-TMS)-xylofuranose, peaks 2, 4 and 5 = unidentified polysaccharides compounds, peak 3 = tri-(O-TMS)-levoglucosane

Layer 2 (red-brown layer) aminoacidic profile was not obtained due to the quantity of sulphates present in the layer. Sulphates are retained in the pre-column and thus no aminoacids are arriving to the mass detector. No more sample was available to be analyzed, thus the aminoacidic content of layer 2 was not characterized.

Layer 3 (green-blue layer) presented a proteinaceous material quantity slightly higher than the blank of the technique. The PCA treatment of the sample aminoacidic profile (Table 5) indicates that the sample cannot be attributed to a cluster but it is situated in between the egg and the casein clusters (Fig. 5). That could be attributed to the high degradation of the proteinaceous material in the sample. The high

Table 5 Amino acidic relative percentage content of layer 3 compared to characteristic values of egg, casein and animal glue

Sample	Ala	Gly	Val	Leu	Ile	Ser	Pro	Phe	Asp	Glu	Hyp
Milk (casein)	5.0	3.0	7.6	11.9	6.6	5.8	11.5	5.9	8.5	22.2	0.0
Egg	7.7	4.8	7.7	11.0	6.7	10.3	5.7	6.4	12.6	15.0	0.0
Animal glue	12.3	29.4	3.9	4.7	2.5	3.8	12.4	2.8	6.6	9.9	7.7
Layer 3	7.1	21.6	8.3	18.1	9.2	2.6	7.6	6.0	5.7	13.9	0.0

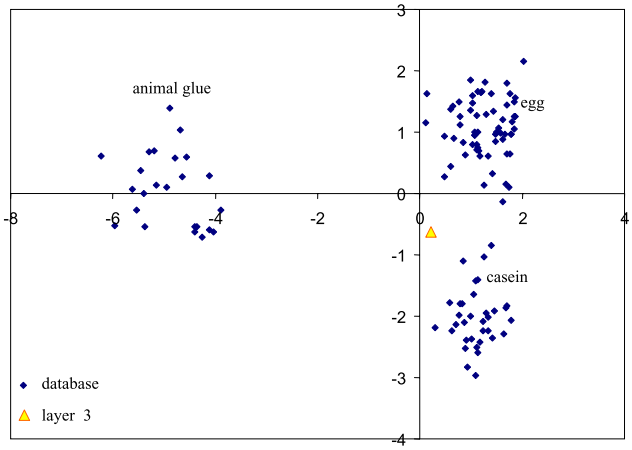

Fig. 5 Principal component analysis score plot of the amino acids percentage relative content in sample E1

Glycine content in the sample could be attributed to a bacterial attack [25]; this could have also generated the low levels of aspartic acid that would justify the sample shift towards the casein cluster.

Besides, the fatty acid composition of layer 3 highlights a profile that is not an oil nor a whole egg one. Characteristic ratios ($A/P = 0.15$, $P/S = 0.8$; $\Sigma D = 5.0$) are not consistent with the ones of a siccative oil, but the content of dicarboxylic acids could suggest the use of an egg undergone to deterioration as binding media. Moreover, an animal fat has been identified due to the presence of pentadecanoic, eptadecanoic, nonanoic acids and their isomers.

2.2.5 Synchrotron radiation FTIR microanalysis

Remaining fragments of the blue layer were prepared for the mapping experiments performed at the ESRF in order to establish the distribution of the compounds already identified. For SR FTIR experiments, sample preparation has been described in a previous work already published [26].

Sample preparation is the key point in order to be able to perform transmission experiments. Due to sample characteristics (low organic material content, high brittleness, large pigment particles) some sample preparation strategies were not applicable. Direct squeezing in a diamond cell or polishing a KBr pellet described in literature [27, 28] result in a complete destruction of the sample or the complete loss of distributional information.

The embedment of the sample in an epoxy resin (spurr) and the microtoming of 10 µm slices give results good enough without loosing distribution information. The infiltration of the resin in the sample was not a real problem as organic materials were almost inexistent (see Sect. 2.2.4) and the inorganic compounds to be studied present characteristic intense bands easily identifiable in the spectra with few overlappings with the embedding resin peaks. Quality of the spectra was good enough for slices from 4 to 10 µm.

The slice selected for the mapping is of 10 µm (Fig. 6) and present some holes due to the microtoming process in the mapped area of 130 µm per 140 µm. A white area corresponding to the presence of layer 1 can be appreciated in the bottom left part of the mapped area next to the hole. The rest of the mapped area corresponds to layer 3 (blue-green layer). Some blue particles can also be appreciated.

The spectra were individually valuated considering three different wavenumber ranges where the embedding media characteristic bands (Table 4) allow identification of some functional groups.

Range 1 (4000–3000 cm^{-1}) allow the identification of the particularly intense stretching OH bands of copper hydroxychlorides and azurite. In this range the resin presents just a not intense resin broad band.

Range 2 (under 1000 cm^{-1}) presents no bands of the embedding media. In this range, CO bending of azurite, C–C of oxalates and C–Cl st of copper hydroxychlorides are displayed. All bands of copper hydroxychlorides occur in the ranges 1 and 2 and their characterization is completely unequivocal.

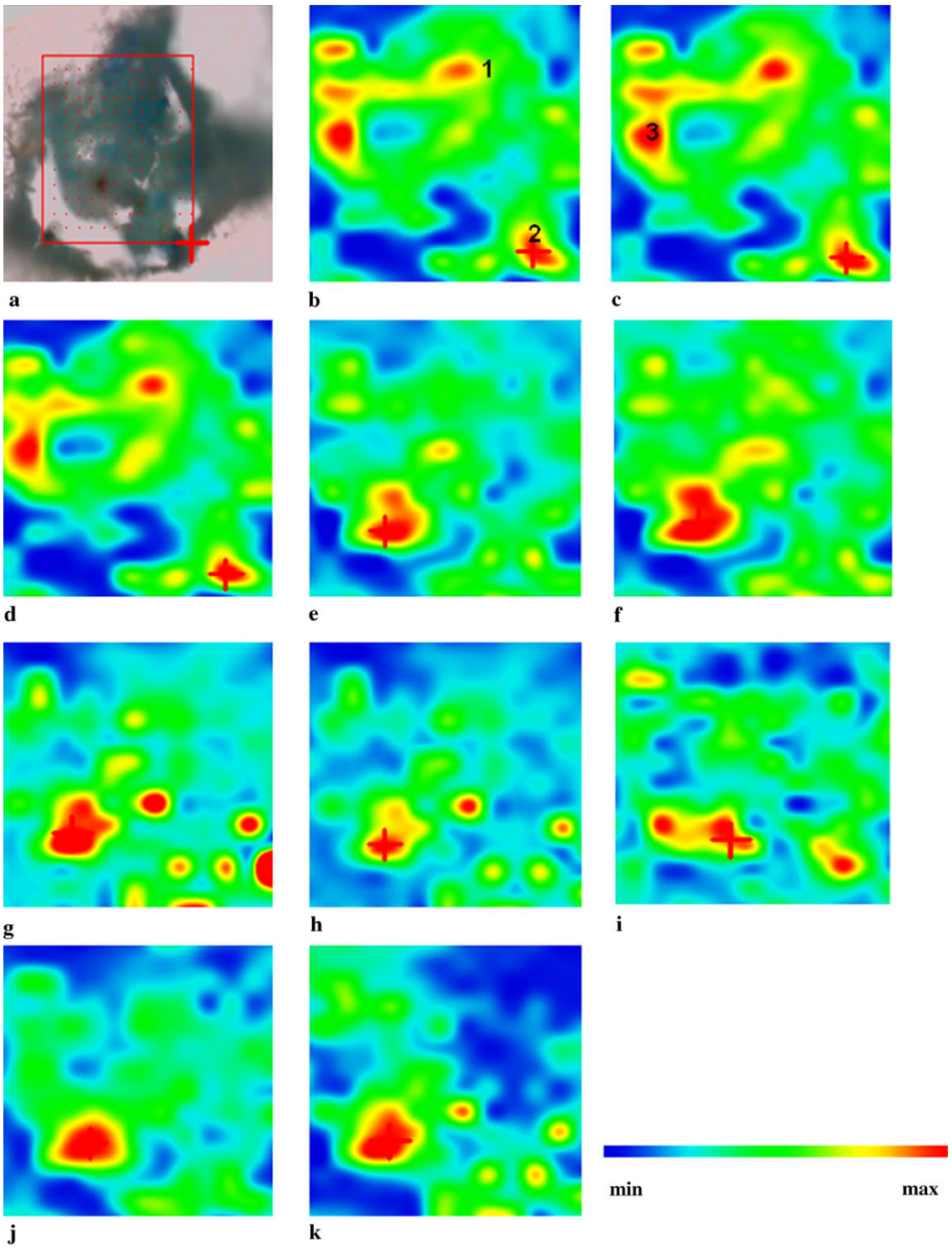

Fig. 6 (**a**) Photomicrograph of the microtomed cross section. The *rectangle* marks the area selected to perform the SR FTIR mapping; chemical image of (**b**) 3428 cm^{-1}, (**c**) 3443 cm^{-1}, (**d**) 3337–3354 cm^{-1}, (**e**) 1320 cm^{-1}, (**f**) 1365 cm^{-1}, (**g**) 825 cm^{-1}, (**h**) 780 cm^{-1}, (**i**) 3541 cm^{-1}, (**j**) 1620–1684 cm^{-1}, (**k**) 1116–1143 cm^{-1}. Mapped area 130 × 140 μm

Range 3 (1700–1000 cm^{-1}) presents different characteristic bands of the embedding media which penetration can be easily noticed by the presence of the CH stretching characteristic bands at 2960, 2935 and 2872 cm^{-1} and the C=O stretching at 1736 cm^{-1}. Their presence immediately indicates that CH stretching and C=O st cannot be used for

Table 6 Bands mapped by SR FTIR imaging experiments

Band mapped (cm^{-1})	Attributed functional group	Material
3540	ν(OH)	Gypsum
3445, 3354–3337	ν(OH)	Hydroxychlorides
3430	ν(OH)	Azurite
1620	ν(HOH), ν(C=O)	Gypsum oxalates
1365	ν(C–O)	Copper oxalates
1320	ν(C–O)	Oxalates
1120	SO_4	Gypsum
825	ν(C–C)	Copper oxalates
780	ν(C–C)	Calcium oxalates

organic material identification and that bands in range 3 (1700–1000 cm^{-1}) should be considered carefully (to avoid confusion with the rest of the bands of the embedding resin in this range).

However, as we can see in Table 4 some characteristic bands of azurite and oxalates are not completely overlapped with those of the embedding media. The intensity of some of the inorganic functional groups absorbance makes some of them easy to be recognized when present, also in the presence of the embedding media bands, due to the characteristic shape or intensity changes respect to the pure embedding resin spectra. Moreover, some of the spectra did not present embedding media interferences at all. Table 6 presents the bands mapped in Fig. 6.

The mappings of the OH stretching bands characteristic of azurite (3430 cm^{-1}), atacamite (3445, 3353 cm^{-1}) and paratacamite (3449, 3360, 3320 cm^{-1}) indicate the same areas of occurrence (higher intensity of the characteristic bands) for all of them (areas 1, 2, 3 in the mappings in Fig. 6).

The spectra of the areas underlined by the mapping (Fig. 7a) present two intense bands in range 1 (4000–3000 cm^{-1}). Those broad bands are centred at 3448 cm^{-1} and 3340 cm^{-1}. The resolution of the experiment of 8 cm^{-1} does not allow one to distinguish between atacamite and paratacamite nor establish the presence of azurite. In fact, reference spectra of both copper hydroxychlorides mixtures give similar results.

The rest of the bands of individual spectra of areas 1, 2, 3 in range 2 (under 1000 cm^{-1}) are 985, 953, 919, 895 cm^{-1} and a broad band at 840 cm^{-1} with a shoulder at 820 cm^{-1}. Those bands mainly correspond to the C–Cl st of atacamite and paratacamite [19]. However, the intensity of the band at 950 cm^{-1} together with the presence of a broad band around 840 cm^{-1} was considered indicative of the presence of azurite. The shoulder at 820 cm^{-1} could also be in correspondence with the C–C bands of copper oxalates although azurite can present a less intense band also at this wavenumber.

In fact, the band at 1321 cm^{-1} of oxalates (CO st) can be easily identified in range 3 (1700–1000 cm^{-1}) together with a band at around 1650 cm^{-1} and a peak at 1365 cm^{-1}. The occurrence of those bands indicates the presence of copper oxalates in those areas.

Moreover, the features of the spectra of area 1, 2, 3 in the range 1500–1400 are not in correspondence with those of the embedding medium reference spectra but resemble those of the characteristic peaks of azurite at 1465 and 1423 cm^{-1} (CO st), in accordance with the bands at 950 and 840 cm^{-1} (CO bd) observed in the same spectra in range 3 (above mentioned). Thus, azurite is mixed together with copper hydroxychlorides and copper oxalates in those areas (areas 1 to 3).

However, when mapping the characteristic bands of oxalates, that is 1320 and 1630 cm^{-1}, a different area (area 4 in Fig. 6) presents major peak intensities. Mapping the specific peaks of copper oxalates (1365 and 825 cm^{-1}) and calcium oxalates (780 cm^{-1}) separately, major intensities coincide again in the same area (area 4). In the spectra of area 4 (Fig. 7 b) all those bands can be identified meaning that probably both kind of oxalates (calcium and copper) are present. In this area none of the peaks of azurite nor copper hydroxychlorides could be detected but other characteristic features were observed.

Range 1 (4000–3000 cm^{-1}) of the spectra of area 4 do not present the intense bands characteristic of hydroxychlorides but different bands corresponding to those of HOH st of oxalates and those of the OH st of gypsum (3540 cm^{-1}). That is in correspondence with the broad band around 1650 cm^{-1} and the presence of a band around 1150 cm^{-1} in those spectra. The broad band at 1650 cm^{-1} is the result of calcium and copper oxalate (1644 cm^{-1}) bands together with those of HOH st of gypsum (1685 and 1620 cm^{-1}) while the peak around 1150 cm^{-1} would correspond to the stretching of the sulphate group. The presence of gypsum in this area is consistent with the preparation layer (layer 1) observed in the microtomed section.

The mappings of the characteristic vibrational bands evidenced in the individual spectra of area 4 are again consistent with the higher absorbance of those vibrational bands mainly in area 4. Thus, oxalates are mainly distributed next to the gypsum layer although they were also present in the areas were azurite and hydroxychlorides were mainly present.

A linescan of the sample, that is representation of a unique series of spectra crossing the sample vertically, thus the wavenumbers versus position graphic, allows for the easy identification of the main spectral treats specified above in a chosen in depth line (Fig. 7). The line selected for the linescan generation, thus considered representative, is depicted in the microtomed section in Fig. 8a. Like in the mappings, some highlighted areas, corresponding to the intense bands in the spectra of that position in the line, are the result of the absorbance of the embedding resin. Those bands

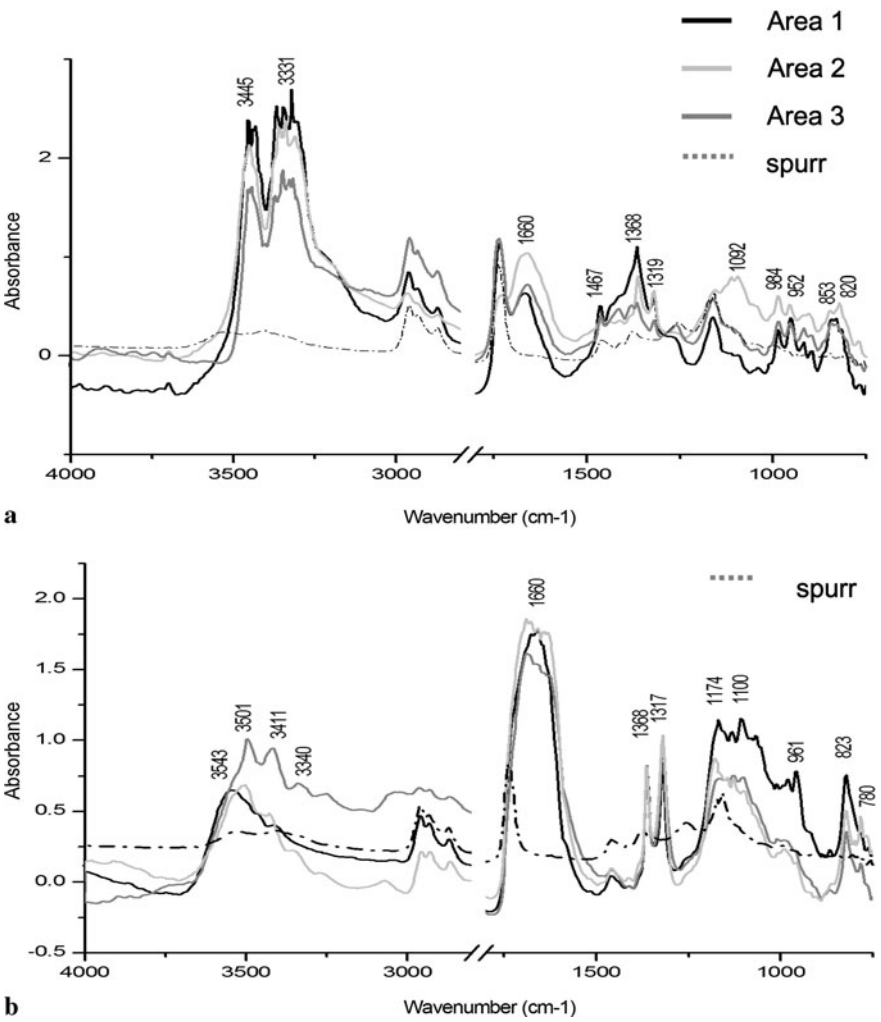

Fig. 7 Selected SR FTIR spectra of the representative areas individuated in the chemical maps in Fig. 6. (**a**) Areas 1, 2, 3 and (**b**) different spectra from area 4

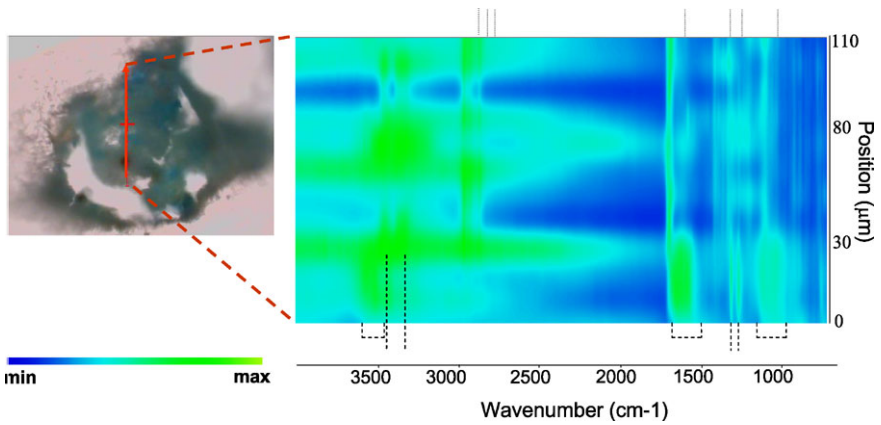

Fig. 8 Photomicrograph of the sample. The *red line* indicates the selected line to perform the linescan. Linescan of the sample. *Grey dotted lines* on top of the linescan indicate the characteristic bands of the embedding resin, while *black dashed lines* on the *bottom* evidence the bands highlighted corresponding to the main features

(specified above and Table 4) are marked with a dotted line in Fig. 7.

The linescan starts in the area correspondent to layer 1 (position 0) and finishes at the end of the microtomed section in layer 3 (position 110). In the bottom of the linescan (spectra 0 to 30, corresponding with area 4) characteristic bands of the OH st of gypsum correspond to a highlighted broad area around 3500 cm^{-1}. Another highlighted area around 1100 cm^{-1} corresponds to the sulfate.

A broad area around 1650 cm^{-1} corresponds to the presence of both HOH st bands of gypsum (1680, 1620 cm^{-1}) and the C=O st of oxalates (1644, 1620 cm^{-1}). This broad band is not present in the scans from 30 to 110 although a narrower band corresponding to C=O st of oxalates is

present in some of the spectra such as scan 80–90. That is consistent with the fact that oxalates were also identified in those areas (area 1, 2, 3) by the valuation of the individual spectra.

Finally, scans from 0 to 30 clearly present two narrow bands corresponding to the copper oxalate characteristic C–O st vibrations at 1359 and 1320 cm^{-1} with similar intensities consistent with the presence of copper oxalate in the spectra of these area and the mapping of the bands presented above. From scan 30 to 110, two different highlighted bands at around 3430 and 3340 cm^{-1} correspond to the OH st of azurite and the hydroxychlorides are highlighted.

2.3 Discussion and interpretation of the measurements

The combined interpretations of results of different techniques allow one to reliably characterize the samples from an organic and inorganic point of view. This way, the composition of the different layers was established.

Although the organic material presents some problematics for its reliable identification, due to its degradation and low amount, the presence of a proteinaceous material in the blue layer and polysaccharide material in both pigment layers seems clearly established. The aminoacidic profile, together with acidic fraction results, allows one to identify the proteinaceous material as egg. Moreover, an animal fat seems also been used as binding media or coating.

Compounds formed as a result of the synthesis of green pigments such as copper acetates or malachite have not been identified which lead to discard the use of a synthetic green mixture of different copper compounds such as the ones described by Teophilus or Heraclius and confirm the degradation hypothesis for the green shades of the blue layer.

The presence of azurite used as blue pigment in the blue layer, and the mixture of copper hydroxychlorides and copper oxalates in the green areas of this layer was clearly established by conventional FTIR. Calcium oxalates were also identified in high amounts in the gypsum ground (layer 1). It should be noticed that both degradation products (hydroxychloride copper and copper oxalates) display green shades which modify the original blue wall-painting.

SR FTIR experiments underlined the presence of hydroxyhlorides and copper oxalates in the blue layer. The products of degradation of azurite (copper hydroxy chlorides) look like being mainly formed on top of the blue pictorial layer far from the gypsum layer 1, suggesting an external source of chloride ions. Azurite is also mixed with copper hydroxy chlorides in those areas. Copper oxalates, although being also present together with azurite and the hydroxychlorides, are concentrated next to the preparation layer where their characteristic peaks are predominant in the spectra. Calcium oxalates are also present in this area maybe due to their high concentration in layer 1 (characterized by conventional FTIR).

Thus, the distribution of degradation by-products (copper hydroxychlorides and oxalates) seems to point out a competition among them: in presence of a source of chlorides the formation of hydroxychloride compounds have a greater yield while in the absence of chlorides (in deeper layers), oxalates formation occur in greater amounts.

Calcium oxalates are often found in most cultural heritage objects exposed at the open air. The origin of calcium oxalates is yet under investigation. A set of researchers claim they have a biological origin by mineralization and collapse of algae filaments [29] while others consider oxalates a catabolic product of micro-organisms colonisations fed by organic materials such as binding media are [30, 31]. A third hypothesis considers a chemical origin as oxidation products of those organic substances applied as conservation treatments and binding media [32, 33].

The key findings achieved by SR imaging techniques on oxalates formation in painting samples until now were the evidence that calcium oxalates could be found not only in the surface but also in layers under gold leaves were organic materials were identified [26]. Thus a relationship among the simultaneous presence of organic material and calcium oxalate seems to be evident.

In this case, the presence of an organic material (egg) as binding media in the blue layer has been unequivocally characterized by means of chromatographic techniques coupled with mass spectrometry (GC/MS). Moreover, not only calcium oxalates but also copper oxalates were founded in the samples. Copper oxalates were formed in the blue pictorial layer (layer 3) where copper is present due to the presence of the pigment azurite, while in the gypsum ground (layer 1) calcium oxalates were formed. Thus, the formation of oxalic acid that combines with calcium or copper depending on their availability in the layer is clearly established.

However, the degradation of the binding media by a bacterial attack does not allow us to establish if oxalic acid has been formed by the direct oxidation of the binding media or as a result of its bacterial degradation or both of them.

Finally, although synchrotron radiation techniques add spatial information to the characterization of the blue layer, that is, to the azurite degradation product distribution, some problematics have been highlighted. Mainly, SR FTIR presents the intrinsic difficulties of a technique that is sensible to functional groups. Thus, unequivocal characterization of the crystalline phases present is not possible.

3 Conclusions

The characterization of the samples highlights the presence of azurite and its degradation products in the blue painting layer. The products of degradation evidenced are mainly copper hydroxychlorides. Copper oxalates were also identified in the blue layer under study. The formation of oxalic

acid due to the bacterial degradation presence of an organic binding media in the blue layer would be the origin for those oxalates.

Moreover, imaging techniques allow one to establish the distribution of azurite and its products of degradation in the blue layer.

As a technique sensible to functional groups, FTIR is clearly limited for the unequivocal characterization of different crystalline phases of the same chemical compound. Thus, other imaging techniques such as SR XRD would be necessary to characterize unequivocally the different phases present and to be able to map them separately.

Acknowledgements Authors wish to thank AGAUR (Agència de gestió d'Ajuts Universitaris I de recerca), acknowledged for the research grant (BE00729) that permitted the stage at the University of Pisa to learn the chromatography procedures and professor M.P. Colombini and Dr. Ilaria Bonaduce of the University of Pisa for their hospitality. This research has been founded by the project HUM2006-06609, from the Spanish Ministry of Education and Research. We also acknowledge the European Synchrotron Radiation Facility for provision of synchrotron radiation facilities as part of the project EC38 (Calcium oxalate formation in mural paintings) and we would like to thank Marine Cotte and Jean Susini for their assistance in using beamline ID21.

References

1. A. Roy, *Artists Pigments: A Handbook of Their History and Characteristics*, vol. 2 (National Gallery of Art, Oxford, 1993)
2. A. Andreotti, I. Bonaduce, M.P. Colombini, C. Baracchini, A. Caleca, A. Paolucci, *Saving the Medieval Paintings by the Master Painter of the Triumph of Death in Pisa in 15th Triennial Conference New Delhi* (Allied Publishers, India, 2008)
3. S. Mugnaini, A. Bagnoli, P. Bensi, F. Doghini, A. Scala, G. Guasparri, J. Cult. Heritage **7**, 171 (2006)
4. C. Cennini, *Il Libro del Arte* (Akal Ediciones, Madrid, 2002)
5. O. Vitruvio, *Los Diez Libros de Arquitectura* (Alianza Forma, Madrid, 2000)
6. M.P. Merrifield, *The Art of Fresco Painting in the Middle Ages and Renaissance* (Dover, New York, 2004)
7. N. Salvadó, T. Pradell, E. Pantos, M.Z. Papiz, J. Molera, M. Seco, M. Vendrell-Saz, J. Synchrotron Radiat. **9**, 215 (2002)
8. P. Vandenabeele, K. Lambert, S. Matiz, W. Schudel, A. Bergmans, L. Monees, Anal. Bioanal. Chem. **383**, 707 (2005)
9. L. Dei, A. Ahle, P. Baglioni, D. Dini, Stud. Conserv. **43**, 80 (1998)
10. I. Bonaduce, M.P. Colombini, J. Chromatogr. A **1028**, 297 (2004)
11. A. Andreotti, I. Bonaduce, M.P. Colombini, G. Gautier, F. Modugno, E. Ribechini, Anal. Chem. **78**(13), 4490 (2006)
12. R.J. Gettens, M.E. Mrose, Stud. Conserv. **1**(4), 174 (1954)
13. C. Genesta, Matter Lett. **54**, 382 (2002)
14. K. Helwig, IRUG at the V&A 83
15. D. Biakiaris, S. Danilia, S. Sotiropoulou, O. Katsimbiri, E. Pavlidou, A.P. Moutsatsou, Y. Chryssoulakis, Spectrochim. Acta A **56**, 3 (1999)
16. A. Nevin, J. Loring Melia, I. Osticioli, G. Gautier, M.P. Colombini, J. Cult. Heritage **9**(2), 154 (2008)
17. E. Abelev, N. Sezin, Y. Ein-Eli, Rev. Sci. Instrum. **76**, 106105 (2005)
18. J. Madejová, Vibr. Spectrosc. **31**(1), 1 (2003)
19. I. Adrover Gracia, *Applicazioni Della Spettrofotometria IR Allo Studio dei Beni Culturali* (Collana I Talenti, Padova, 2001)
20. R.L. Frost, Y. Jing, Z. Ding, Chin. Sci. Bull. **48**(17), 1844 (2003)
21. M.C. D'Antonio, D. Palacios, L. Coggiola, E.J. Baran, Spectrochim. Acta, Part A **68**(3), 424 (2007)
22. S. Bruni, F. Cariati, F. Casadio, L. Toniolo, Vibr. Spectrosc. **20**, 15 (1999)
23. A. Andreotti, I. Bonaduce, M.P. Colombini, F. Modugno, E. Ribechini, Int. J. Mass Spectrom. (2008). ISSN 1387-3806
24. G. Gautier, M.P. Colombini, Talanta **73**, 95 (2007)
25. I. Donati, Enzimi, acidi organici ed altri metaboliti coinvolti nella patogenesi di penicillium spp. PhD thesis, Universita di Bologna Italy (2008)
26. A. Lluveras, S. Boularand, J. Roqué, M. Cotte, G. Martinez-Ruiz, P. Giráldez, M. Vendrell-Saz, Appl. Phys. A **90**(1), 23 (2008)
27. M. Cotte, J. Susini, V.A. Solé, Y. Taniguchi, J. Chillida, E. Checroun, P. Walter, J. Anal. At. Spectrom. **23**, 820 (2008)
28. J. van der Weerd, R.M.A. Heeren, J.J. Boon, Stud. Conserv. **49**, 193 (2004)
29. M. Garcia-Vallès, M. Vendrell-Saz, J. Molera, F. Blázquez, Environ. Geol. **36**, 137 (1998)
30. J.K. Magnuson, L.L. Lasure, *Advances in Fungal Biotechnology for Industry, Agriculture, and Medicine* (Kluwer Academic/Plenum, Norwell/New York, 2003)
31. M.V. Dutton, C.S. Evans, Can. J. Microbiol. **42**, 881 (1996)
32. F. Cariati, L. Rampazzi, L. Toniolo, A. Pozzi, Stud. Conserv. **45**, 180 (2000)
33. P. Maravelaki-Kalaitzaki, Anal. Chim. Acta **532**, 187 (2005)